



TITLE:

# Investigation of self-sealing in high-strength and ultra-low-permeability concrete in water using micro-focus X-ray CT

AUTHOR(S):

Fukuda, Daisuke; Nara, Yoshitaka; Kobayashi, Yuya; Maruyama, Megumi; Koketsu, Mayuko; Hayashi, Daisuke; Ogawa, Hideo; Kaneko, Katsuhiko

---

CITATION:

Fukuda, Daisuke ...[et al]. Investigation of self-sealing in high-strength and ultra-low-permeability concrete in water using micro-focus X-ray CT. Cement and Concrete Research 2012, 42(11): 1494-1500

ISSUE DATE:

2012-11

URL:

<http://hdl.handle.net/2433/162005>

RIGHT:

© 2012 Elsevier Ltd.; This is not the published version. Please cite only the published version.; この論文は出版社版ではありません。引用の際には出版社版をご確認ご利用ください。

4 Daisuke FUKUDA<sup>1</sup>, Yoshitaka NARA<sup>2</sup>, Yuya KOBAYASHI<sup>3</sup>, Megumi  
5 MARUYAMA<sup>1</sup>, Mayuko KOKETSU<sup>1</sup>, Daisuke HAYASHI<sup>4</sup>, Hideo OGAWA<sup>5</sup>,  
6 Katsuhiko KANEKO<sup>6</sup>

<sup>3</sup> Graduate School of Engineering, Hokkaido University, Kita 13 Nishi 8, Kita-ku, Sapporo, Hokkaido 060-8628, Japan (Present address: Tokyo Gas Co. Ltd., 5-16-20 Kita Urawa, Urawa-ku, Saitama 330-0074, Japan)

14 <sup>4</sup>Taiheiyo Consultant Co., Ltd., Ohsaku, Sakura 285-8655, Japan (Present address:  
15 Radioactive Waste Management Funding and Research Center, Tsukishima 1-  
16 15-7, Chuo-ku, Tokyo, 104-0052, Japan)

17 <sup>5</sup>Taiheiyo Consultant Co., Ltd., Ohsaku, Sakura 285-8655, Japan

<sup>6</sup> Faculty of Engineering, Hokkaido University, Kita 13 Nishi 8, Kita-ku, Sapporo,  
Hokkaido 060-8628, Japan

21      \*Corresponding author: Yoshitaka NARA

22 E-mail: nara.yoshitaka.2n@kyoto-u.ac.jp

23 TEL&amp;FAX: +81-75-383-3211

Key words: crack, self-sealing, micro-focus X-ray CT, image subtraction, high-strength and ultra-low-permeability concrete

29    **Abstract**

30

31    High-strength and ultra-low-permeability concrete (HSULPC) is thought to be  
32    useful as a radioactive waste package. Thus, a high confining ability is desirable.  
33    For cementitious materials, sealing of cracks may occur in water due to the  
34    precipitation of calcium compounds. This can affect the confining ability. In this  
35    study, the sealing of a crack in HSULPC in water was investigated using micro-  
36    focus X-ray computed tomography (CT). The sealing by precipitation occurred  
37    only around the end of the specimen. Sealed regions of the crack were identified  
38    using three-dimensional image registration and CT image subtraction of images  
39    obtained for the specimen before and after it was immersed in water to evaluate  
40    temporal changes of the sealing deposits in the crack. The sealing deposits  
41    increased as the HSULPC specimen was kept in water longer. It was concluded  
42    that cracks in HSULPC in water are sealed by precipitation.

## 1. Introduction

For the geological disposal of radioactive wastes, the radioactivity intensity of the radionuclides can be reduced by engineered barriers, such as bentonite buffers, and natural barriers, such as rock mass. If a repository of radioactive waste is located in an area where the hydraulic gradient and the permeability are high, the retardation of radionuclide migration by these barriers may not be sufficient. To retard the migration, several alternative concepts of radioactive waste packages are being developed. High-strength and ultra-low-permeability concrete (HSULPC) is planned for radioactive waste packages for the geological disposal of transuranic (TRU) waste [1–3] to confine the radionuclides with low adsorption by the engineered barriers, such as C-14 included in TRU waste in Japan.

Generally, water migrates through networks of cracks and pores in a solid. In cementitious materials, precipitation, mainly of calcium compounds, occurs in water. Thus, the sealing of cracks and pores by precipitation can occur, and this may affect permeability. This phenomenon has been investigated by various researchers [4–12]. Edvardsen [7] showed that sealing of a crack occurs by precipitation of calcium carbonate, generated from  $\text{CO}_3^{2-}$  in water and  $\text{Ca}^{2+}$  in cement paste. The crack width and applied water pressure affected the sealing significantly, but the composition of the surrounding water had little effect [7]. Yang et al. [11] showed that sealing occurs if the crack width is less than 0.15 mm. Reinhardt and Jooss [8] investigated the temperature dependence of the sealing and showed that sealing is enhanced with increasing temperature, up to 80°C.

Because a high confining ability is required for HSULPC, detailed investigation of the sealing of cracks and pores in water is of considerable importance. It is thus important to observe the sealing of cracks and pores directly. X-ray computed tomography (CT) scanners are an effective tool for observing the sealing of cracks and pores, because we can observe not only the surface but also the interior of the material with this non-destructive technique. Specifically, we can observe the details of the sealing of cracks and pores in HSULPC using micro-focus X-ray CT, because images with high resolution can be obtained. However, to date, observations of this sort have not been reported. Additionally, the temporal behavior of sealing has not yet been clarified.



77        In this study, we investigated the sealing of cracks in HSULPC in water using  
78    micro-focus X-ray CT.

79    **2. Sample**

80

81        HSULPC made by Taiheiyo Co., Ltd., was used. Because detailed information  
82        about the material properties of HSULPC has been reported previously by Nara et  
83        al. [13], we provide only the composition of the HSULPC in Table 1.

84        Fig. 1 shows a photograph of the cracked HSULPC specimen used in this  
85        study. An initially intact cylindrical specimen of HSULPC was split in half axially  
86        using the Brazil test technique, and was set in an acrylic cylinder tube. The initial  
87        crack width was approximately 0.1 mm throughout the specimen. The height of  
88        the acrylic cylinder tube was 35 mm. The diameter and height of the HSULPC  
89        specimen were approximately 13 mm and 15 mm, respectively.

### 90 3. Observation by X-ray CT

91

#### 92 3.1. Observation method

93

94 In Japan, salt water is often found underground [14–16]. Thus, considering the  
95 condition of groundwater in Japan, the HSULPC specimen was kept in simulated  
96 seawater inside a plastic bottle. Table 2 shows the chemical composition of the  
97 simulated seawater used. When the specimen was kept in water, a vacuum  
98 desiccator was used to ensure that water would fill the entire crack. The amount  
99 (weight) of water used was ten times larger than the weight of the HSULPC  
100 specimen. To avoid the undesirable dissolution of CO<sub>2</sub> in the water, the air in the  
101 plastic bottles was replaced with nitrogen gas. The specimen was kept in a  
102 thermostatic chamber at a temperature of 293 K. Because X-rays are more or less  
103 attenuated by the presence of water and this causes undesirable error in the image  
104 analysis, as discussed below, the HSULPC specimen was dried for a day at room  
105 temperature before each X-ray CT observation so as to remove the water from the  
106 specimen. The observations were conducted at the start and after keeping the  
107 specimen in water for 1, 3, and 7 weeks.

108 For the observation by X-ray CT, a micro-focus X-ray CT scanner,  
109 TOSCANER 31300μhd (Toshiba IT & Control Systems Co., Ltd.), installed at  
110 Hokkaido University, Japan, was used. The applied tube voltage and maximum  
111 tube current were 130 kV and 62 μA, respectively, which were used in each scan  
112 in this study. For X-ray CT scanning, cone-beam scanning mode [17] was used in  
113 which multiple CT images, up to several hundred cross sections, were provided  
114 through one scan, and quick three-dimensional (3D) reconstruction of specimen  
115 was possible. The number of pixels in each cross section was 1024 × 1024  
116 corresponding to 16 μm × 16 μm for each pixel. The notion of a “voxel” is used in  
117 X-ray CT, defined as a pixel having some thickness, named the slice thickness.  
118 Here, the slice thickness was 24 μm.

119 During scanning, the observed specimen is placed on a table and the table  
120 rotates continuously with the relative positions between the X-ray tube and  
121 detector, named an X-ray image intensifier, being fixed. The number of projection  
122 directions used in all scans was 1500 (i.e., the interval between each projection  
123 angle was 2π/1500 radians). In each projection direction, 20 consecutive scans

were conducted and averaged projection data were used for image reconstruction to reduce statistical noise caused in the X-ray image intensifier. The linear attenuation coefficient [18],  $\mu$ , for each voxel was computed from the projection data with an image reconstruction algorithm, based on a filtered back-projection method [17, 19] in which a Ramachandran-Lakshminarayanan filter function [20] was used. Then, CT images were reconstructed through the CT values, calculated as follows:

$$V_{\text{ct}} = S\mu + B \quad (1)$$

where  $V_{\text{ct}}$  is the CT value, which is a signed integer taking a value between  $-8192$  and  $8191$ , and  $S$  and  $B$  are both constants. In this study,  $S$  and  $B$  were  $200$  and  $0$ , respectively. The CT values in Eq. (1) are not defined in Hounsfield units, as found in many industrial X-ray CT scanners. For noise reduction measures, which are quite important in X-ray CT, a reduction in undesirable effects of scattered X-rays on the X-ray image intensifier was achieved using an X-ray collimator set in front of X-ray tube. Additionally, two notorious artifacts, the cupping effect, due to beam hardening, and the ring artifact [17, 18], were minimized using a copper filter with a thickness of  $0.1$  mm in a so-called “gain calibration” [18].

Based on the considerations above,  $680$  CT slice images in total were obtained to reconstruct the entire crack in the HSULPC specimen by X-ray CT scanning and to identify the precipitated regions.

### 3.2. Results

A typical CT slice image at one cross section of the specimen before it was kept in seawater is shown in Fig. 2. The cross section also corresponds to the top in the image analysis described in Section 4. Based on a window level of  $400$  and a window width of  $1200$ , this image is presented in gray-scale with a range of  $256$  shades from black to white. High CT values, shown in white or brighter colors, correspond to regions with higher density. Regions of low CT values, shown in black or darker colors, correspond to areas of lower density. The black zigzag line found in the central part of the image is the crack, and the dark circular shapes of various sizes are pores. Small white granular regions having higher density are also found over the whole slice and these correspond to metal included in the

158 silica fume as a byproduct of metal refining. The other regions, shown in gray  
159 colors, are the matrix of HSULPC, consisting of cement and aggregates.

160 It was observed from the CT images that most of the pores with their diameters  
161 approximately greater than ten micrometers were isolated from each other,  
162 although some of the pores were on the surface of the specimen. Additionally,  
163 some pores were connected to the crack. It may be possible that pores of much  
164 smaller sizes ( $< 1 \mu\text{m}$ ) are connected, which are not observable at the resolution of  
165 the used CT scanner. Fig. 3 shows CT images of the crack, for approximately the  
166 same cross section, extracted from seven CT images of a specimen before it was  
167 immersed in seawater and after it was kept in seawater for 7 weeks. These images  
168 are presented at intervals of  $48 \mu\text{m}$  from one end to the interior of the specimen. In  
169 the region close to the end, most parts of the crack were sealed in the HSULPC  
170 specimen kept in seawater for 7 weeks. In contrast, less sealing was observed  
171 towards the interior of the specimen. Although most parts were sealed in the crack  
172 closer to the end, the CT image of the corresponding part showed blurring due to  
173 the so-called “partial volume effect” [18], where voxels are affected by including  
174 both precipitates and air within them. Blurring is also caused by the tilted surface  
175 of the specimen at the ends. From these results, sealing of the crack by  
176 precipitation generally occurred only near the end of the specimen.

177 Fig. 4 shows the temporal change in sealing of the crack for one cross section.  
178 These cross sections are the same sections as Fig. 2 and those indicated by dotted  
179 lines in Fig. 3(a). The occurrence of precipitation was observed after the specimen  
180 was kept in water for 1 week. Additionally, the sealed area increased with elapsed  
181 time. Because no re-opening of the sealed crack was found, dissolution of the  
182 precipitates did not occur over the period of observation. No swelling of the  
183 specimen was found during the period of observation.

184 The following observations were clarified by the X-ray CT. The occurrence of  
185 significant precipitation was found from the end to the interior of the specimen  
186 within a range of approximately  $0.2 \text{ mm}$ , and the total amount of precipitate  
187 increased with elapsed time in the region closer to the end. Most parts of the crack  
188 were sealed after 7 weeks due to precipitation near the end. Once such sealing was  
189 achieved, no further precipitation was observed in the crack below the sealed part.

190 A photograph of the end of the specimen kept in seawater is shown in Fig. 5.  
191 Precipitation occurred in such a way that the precipitates covered over the end.

192       Based on these results, image analyses were conducted to evaluate the sealing  
193   process only near the end of the specimen, where significant precipitation was  
194   observed in the crack.

## 4. Image analysis

### 4.1 Image processing method

To investigate temporal changes in the sealed regions of the crack, it was necessary to extract the sealed regions by image processing. For the cross sections where sealing was observed, we sought to extract precipitates by applying an image subtraction technique between the CT images before and after the specimen was kept in water. However, due to the need to set the specimen on the table in the CT scanner manually before each scan, an alignment gap between the comparison images occurred. Thus, before conducting the image subtraction, image registration was used to minimize the alignment gap. For this purpose, an affine linear transformation, expressed by the following equation, was used:

$$u_i = \alpha_{i1} + \alpha_{i2} \cdot x + \alpha_{i3} \cdot y + \alpha_{i4} \cdot z \quad (i = 1, 2, 3) \quad (2)$$

where  $u_i$  indicates the alignment gap of corresponding voxels between comparison images in three directions, defined in Cartesian coordinates, and  $(x, y, z)$  indicate the integer coordinates of each voxel in the reference CT images. CT images before the specimen was kept in water were used as the reference images, and CT images after the specimen was kept in water were mapped onto the reference integer coordinates. In each direction, four unknown coefficients,  $\alpha_{ij}$ , need to be determined.

Here, we explain how to determine  $\alpha_{ij}$ . In Fig. 6, a 3D image of the upper half of a HSULPC specimen kept in seawater is shown. Distinctly white granular regions are included in the image. We used these granular regions to determine  $\alpha_{ij}$ . The region of interest (ROI) was set as a rectangular parallelepiped. The thickness corresponding to 30 slices from the end to the interior of the specimen was included. The matrix size of the ROI was  $342 \times 342$  in the center of each slice. In the ROI of reference images, 11 sampling points were selected where the white granular regions took their local maximum values. Then, approximate values of  $u_i$  in Eq. (2) for the 11 points were obtained by a least squares method. Then, to obtain more precise values of  $\alpha_{ij}$ , the volumetric cross-correlation,  $C$ , defined in the following equation was introduced:

$$C = \iiint_{\text{ROI}} f_0(x, y, z) \cdot f_R(x + u_1, y + u_2, z + u_3) dx dy dz \quad (3)$$

where  $f_0$  is the spatial distribution of CT values in the reference images and  $f_R$  is that of comparison images, transformed by  $u_i$  of the given  $\alpha_{ij}$ . We considered that  $\alpha_{ij}$  became optimal when  $C$  took the maximum value in the ROI. Because the nearest cross section to the end resulted in blurred CT images (see Fig. 3) and they might cause significant error in the image analysis, blurred CT images were excluded from the top of the ROI. Consequently, the top cross sections of the ROI were those surrounded by dashed lines in Fig. 3(a).

## 4.2 Results

The results of the image subtraction (i.e., subtraction images) are shown in Fig. 7. The reference images correspond to those obtained for the initial specimen before immersion in seawater. Comparison images were obtained after 1, 3, or 7 weeks in seawater. In the figure, only the cracks in the ROI are presented at an interval of 48  $\mu\text{m}$  from the top to the interior of the ROI. These images are displayed in gray-scale, with a range of 256 shades from black to white, for a window level and width of 0 and 1000, respectively. In regions where no change occurred, the difference between the CT values was approximately zero, displayed as a gray color in the subtraction images. In regions where precipitation occurred, the difference between the CT values was positive, displayed as a white color. Fig. 7 shows that the region of precipitation observed in Fig. 3 was successfully extracted from the crack.

In the subtraction images, reasonable segmentation between precipitated and non-precipitated regions was required. If a voxel includes both phases (i.e., precipitated and non-precipitated regions), the CT value, and, accordingly, differences in CT values, of this voxel takes an intermediate CT value between these two phases. Such a voxel is called a “mixel” [21-24]. Based on this, a maximum likelihood thresholding method considering the effect of mixels [21–23] was used to set an appropriate threshold,  $t$ . The threshold was determined from the histogram obtained in the boxed area  $A_t$  in Fig. 8(a). Fig. 8(a) shows the same cross section surrounded by dashed lines in Fig. 7(c). The histogram of the probability density function is shown in Fig. 8(b). The threshold determined from the maximum likelihood thresholding method was  $t = 182$ . Binarized images obtained from the subtraction images in Fig. 7 using this threshold are shown in



262 Fig. 9. The images show the cross sections from the top to the interior of the ROI  
263 at an interval of 48  $\mu\text{m}$ , and demonstrate that the geometry of the precipitate was  
264 successfully segmented using the threshold.

## 5. Discussion

The X-ray CT observation results in Section 3 showed that sealing of the crack by precipitation occurred only near the end of the crack in the specimen. In this region, most parts were sealed. This suggests that the crack near the ends was in an environment where precipitation of calcium compounds, such as calcium carbonate, was enhanced by the calcium ions dissolved from the HSULPC and both the carbonate and bicarbonate ions found in the seawater.

If the crack is completely sealed near the end, the network of cracks inside the HSULPC can be isolated from the surrounding environment, which can cause a decrease in permeability [25] and retard degradation in terms of the confining ability of the HSULPC. Because the CT observations suggest that the sealed regions spread with elapsed time, an investigation of the temporal change of the sealing deposits could provide important information to evaluate the effect of the precipitates on limiting water flow into HSULPC. Thus, we investigated the temporal change of the sealing deposits in the crack.

The 30 binarized images obtained in the previous section were used to evaluate the sealing. Fig. 10 shows a schematic illustration of precipitation in the crack. The percentage of sealing deposits in the crack,  $P_{\text{seal}}$ , in each slice, having slice thickness  $T_{\text{slice}}$ , was calculated.  $P_{\text{seal}}$  was calculated as follows:

$$P_{\text{seal}} = \frac{T_{\text{slice}} S_{\text{pre}}}{T_{\text{slice}} S_{\text{crack}}} \times 100 = \frac{l^2 N_{\text{pre}}}{l^2 N_{\text{crack}}} \times 100 = \frac{N_{\text{pre}}}{N_{\text{crack}}} \times 100(\%) \quad (4)$$

where  $T_{\text{slice}}$  is the slice thickness,  $S_{\text{pre}}$  is the total area of precipitates,  $S_{\text{crack}}$  is the total area of the crack,  $l$  is the pixel size (16  $\mu\text{m}$ ), and  $N_{\text{pre}}$  and  $N_{\text{crack}}$  are the numbers of pixels for precipitates and the crack, respectively, in ROI<sub>1</sub> in Fig. 9.  $N_{\text{pre}}$  in ROI<sub>1</sub> was obtained from the extracted precipitates in the binarized images.  $N_{\text{crack}}$  was obtained by counting the number of pixels corresponding to the crack in ROI<sub>1</sub> by applying the maximum likelihood thresholding method to the reference CT images before the specimen was kept in water, where the regions of the crack and matrix of the HSULPC were segmented. Because the mean value of the crack width in ROI<sub>1</sub> was approximately constant, the temporal change in  $P_{\text{seal}}$ , denoted as  $V_{\text{seal}}$ , was computed using the following equation:

$$V_{\text{seal}} = \frac{\Delta P_{\text{seal}}}{\Delta t} (\% \cdot \text{day}^{-1}) \quad (5)$$

297 where  $\Delta P_{\text{seal}}$  is the change in  $P_{\text{seal}}$  over the given immersion period,  $\Delta t$ .

298  $P_{\text{seal}}$  in ROI<sub>1</sub> is shown in Fig. 11 with respect to the depth from the top to the  
299 interior of ROI<sub>1</sub>. From this figure,  $P_{\text{seal}}$  became larger towards the end in each  
300 period, and  $P_{\text{seal}}$  within a depth of 0.05 mm also increased with elapsed time.

301 Similarly,  $V_{\text{seal}}$  in ROI<sub>1</sub> is shown in Fig. 12 with respect to the depth from the  
302 top to the interior of ROI<sub>1</sub>. From this figure,  $V_{\text{seal}}$  towards the end became larger  
303 than in the inner region. The maximum  $V_{\text{seal}}$  was found at 3 weeks, after which  
304  $V_{\text{seal}}$  started to decrease. This suggests that little sealing could be expected to  
305 occur after 7 weeks in ROI<sub>1</sub>.

306 Based on the investigations described above, when HSULPC is kept in water,  
307 precipitation, such as of calcium compounds, occurs in the crack near the end, and  
308 the sealed regions or sealing deposits increase with elapsed time. Considering the  
309 application of HSULPC, it is desirable that such sealing should occur over a short  
310 period time. Thus, identifying optimum water conditions and crack widths is of  
311 considerable importance. To achieve this, more detailed investigation regarding  
312 the influence of water conditions on sealing and the change in water content due  
313 to precipitation could also be important. Additionally, considering that the  
314 temperature in the surrounding environment changes and that heat release occurs  
315 due to the exothermic reactions of radioactive waste, the temperature-dependency  
316 of the sealing behavior also needs to be further investigated. However, these  
317 investigations are beyond the scope of the present study, and we regard them as  
318 future work. The results reported in this paper could be important for engineering  
319 projects such as the geological disposal of radioactive wastes, and further  
320 accumulation of relevant information is important.

321 **5. Conclusions**

322

323       Sealing of crack in HSULPC was investigated in this study. A cracked  
324       HSULPC specimen was prepared and kept in simulated seawater for up to  
325       7 weeks. The surface and interior of the cracked HSULPC specimen were then  
326       observed using micro-focus X-ray CT.

327       The results revealed that sealing of the crack occurred only near the end of the  
328       specimen. The occurrence of significant precipitation was found within  
329       approximately 0.05 mm from the end.

330       Temporal changes in sealing in the crack showed that the sealing deposits  
331       increased with the time the specimen was kept in water. Additionally, the sealing  
332       deposits increased towards the end of the HSULPC specimen.

333 **Acknowledgements**

334

335       DF was supported by research fellowships from the Japan Society for the  
336       Promotion of Science for Young Scientists. We also appreciate the help and  
337       advice from the Radioactive Waste Management Funding and Research Center.

338 **References**

339

- 340 [1] T. Kawasaki, H. Asano, H. Owada, A. Otsuki, T. Yoshida, T. Matsuo, K.  
341 Shibuya, A. Takei, Development of waste package for TRU-disposal(4) –  
342 Evaluation of confinement performance of TRU waste package made of  
343 high-strength and ultra low-permeability concrete-, Proceedings of GLOBAL  
344 2005, Tsukuba, Japan, Oct. 2005, Paper No. 254.
- 345 [2] H. Owada, A. Otsuki, H. Asano, Development of waste package for TRU-  
346 disposal(1) – Concepts and performances, Proceedings of GLOBAL 2005,  
347 Tsukuba, Japan, Oct. 2005, Paper No. 351.
- 348 [3] K. Shibuya, H. Asano, H. Owada, A. Otsuki, T. Kawasaki, T. Yoshida, T.  
349 Matsuo, A. Takei, Development of waste package for TRU-disposal(3) -  
350 Examination of manufacturing technique of TRU waste package made of  
351 high-strength and ultra low-permeability concrete-, Proceedings of GLOBAL  
352 2005, Tsukuba, Japan, Oct. 2005, Paper No. 256.
- 353 [4] S. Jacobsen, E.J. Sellevold, Self healing of high strength concrete after  
354 deterioration by freeze/thaw, Cem. Concr. Res. 26 (1996) 55–62.
- 355 [5] N. Hearn, C.T. Morley, Self-sealing property of concrete – Experimental  
356 evidence, Mater. Struct. 30 (1997) 404–411.
- 357 [6] N. Hearn, Self-sealing, autogenous healing and continued hydration: What is  
358 the difference?, Mater. Struct. 31 (1997) 563–567.
- 359 [7] C. Edvardsen, Water permeability and autogenous healing of cracks in  
360 concrete, ACI Mater. J. 96 (1999) 448–455.
- 361 [8] H. Reinhardt, M. Jooss, Permeability and self-healing of cracked concrete as a  
362 function of temperature and crack width, Cem. Concr. Res. 33 (2003)  
363 981–985.
- 364 [9] S. Granger, A. Loukili, G. Pijaudier-Cabot, G. Chanvillard, Experimental  
365 characterization of the self-healing of cracks in an ultra high performance  
366 cementitious material: Mechanical tests and acoustic emission analysis, Cem.  
367 Concr. Res. 37 (2007) 519–527.
- 368 [10] S. Qian, J. Zhou, M.R. de Rooij, E. Schlangen, G. Ye, K. van Breugel, Self-  
369 healing behavior of strain hardening cementitious composites incorporating  
370 local waste materials, Cem. Concr. Compos. 31 (2009) 613–621.

- 371 [11] Y. Yang, M.D. Lepech, E.H. Yang, V.C. Li, Autogenous healing of  
372 engineered cementitious composites under wet-dry cycles, *Cem. Concr. Res.*  
373 39 (2009) 382–390.
- 374 [12] T.H. Ahn, T. Kishi, Crack Self-healing behavior of cementitious composites  
375 incorporating various mineral admixtures, *J. Adv. Concr. Technol.* 8 (2010)  
376 171–186.
- 377 [13] Y. Nara, M. Takada, D. Mori, H. Owada, T. Yoneda, K. Kaneko, Subcritical  
378 crack growth and long-term strength in rock and cementitious material, *Int. J.*  
379 *Fract.* 164 (2010) 57–71.
- 380 [14] M. Mizukami, H. Sakai, O. Matsubaya, Na-Ca-Cl-SO<sub>4</sub>-type submarine  
381 formation waters at the Seikan undersea tunnel, Japan. Chemical and isotopic  
382 documentation and its interpretation, *Geochim. Cosmochim. Acta* 41 (1977)  
383 1201–1212.
- 384 [15] T. Iwatsuki, R. Furue, H. Mie, S. Ioka, T. Mizuno, Hydrochemical baseline  
385 condition of groundwater at the Mizunami underground research laboratory  
386 (MIU), *Appl. Geochem.* 20 (2005) 2283–2302.
- 387 [16] K. Hama, T. Kunimaru, R. Metcalfe, A.J. Martin, The hydrogeochemistry of  
388 argillaceous rock formations at the Horonobe URL site, Japan, *Phys. Chem*  
389 *Earth* 32 (2007) 170–180.
- 390 [17] T.M. Buzug, *Computed Tomography: From Photon Statistics to Modern*  
391 *Cone-Beam CT*, first ed., Springer, New York, United States of America,  
392 2008.
- 393 [18] R.A. Ketcham, W.D. Carlson, Acquisition, optimization, and interpretation  
394 of X-ray computed tomographic imagery: Applications to the geosciences,  
395 *Comput. Geosci.* 27 (2001) 381–400.
- 396 [19] A.C. Kak, M. Slaney, *Principles of Computerized Tomographic Imaging*,  
397 Society for Industrial and Applied Mathematics, Philadelphia, Pennsylvania,  
398 United States of America, 2001.
- 399 [20] G.N. Ramachandran, A.V. Lakshminarayanan, Three-dimensional  
400 reconstruction from radiographs and electron micrographs: Application of  
401 convolutions instead of Fourier transforms, *Proc. Natl. Acad. Sci. U.S.A.* 68  
402 (1971) 2236–2240.

- 403 [21] A. Kitamoto, M. Takagi, Estimating the Area Proportions of Mixels Using  
404 Mixture Density Estimation with Mixel Densities: Trans. IEICE, J81-D-II  
405 (1998) 1160–1172 (in Japanese with English abstract).
- 406 [22] A. Kitamoto, A maximum likelihood thresholding methods considering the  
407 effect of mixels, Technical Report of IEICE (Institute of Electronics,  
408 Information, and Communication Engineers), Vol. PRMU99-166 (1999)  
409 7–14 (in Japanese with English abstract).
- 410 [23] A. Kitamoto, M. Takagi, Image classification using probabilistic models that  
411 reflect the internal structure of mixels, Anal. Appl. 2 (1999) 31–43.
- 412 [24] H.S. Choi, D.R. Haynor, Y. Kim, Partial volume tissue classification of  
413 multichannel magnetic resonance images – A mixel model, IEEE Trans.  
414 Med. Imaging 10 (1991) 395–407.
- 415 [25] Y. Gueguen, J. Dienes, Transport properties of rocks from statistics and  
416 percolation, Math. Geol. 21 (1989) 1–13.



## Figure legends

418

419 Fig. 1. Photograph of a cracked HSULPC specimen. The height and diameter of  
420 the HSULPC were 15 mm and 13 mm, respectively. The crack width was  
421 0.1 mm. (a): General view, (b): top view.

422 Fig. 2. X-ray CT sliced image of a cracked HSULPC specimen before it was kept  
423 in seawater.

424 Fig. 3. Comparison of corresponding CT images of the crack: (a): before  
425 immersion in seawater, (b): after it was kept in seawater for 7 weeks. The  
426 height and width of each image are 11 mm and 1 mm, respectively.

427 Fig. 4. Comparison of CT images for a particular section. The height and width of  
428 each image are 11 mm and 1 mm, respectively.

429 Fig. 5. Photograph of precipitation that occurred over the end of the HSULPC  
430 specimen when it was kept in seawater. The regions with the white  
431 coloration correspond to precipitates.

432 Fig. 6. 3D CT image of the upper half of the HSULPC specimen used in the  
433 image analysis, where the ROI used in the image registration given by  
434 Eqs. (2) and (3) is indicated by the rectangular parallelepiped.

435 Fig. 7. Subtraction between the initial reference image and ones obtained after the  
436 specimen was kept in seawater for (a) 1, (b) 3, or (c) 7 weeks. The height  
437 and width of each subtraction image are 3.04 mm and 0.64 mm,  
438 respectively.

439 Fig. 8. Subtraction image and histogram for probability density of CT values used  
440 to determine a threshold. (a) Subtraction image. Region  $A_t$  was used to  
441 determine the threshold segmenting the precipitated and non-precipitated  
442 parts. (b) Histogram obtained from  $A_t$ , where the threshold was  
443 determined from the maximum likelihood thresholding method  
444 considering the effect of mixels.

445 Fig. 9. Binarized images obtained for the differences between reference images  
446 and images after the specimen was kept in seawater for (a) 1, (b) 3, and  
447 (c) 7 weeks. The height and width of each subtraction image are 3.04 mm  
448 and 0.64 mm, respectively. The crack width in  $ROI_1$  was 0.06 mm.

449 Fig. 10. Schematic diagram of precipitation on the surface of the crack in each  
450 slice.

- 451 Fig. 11. Relationship between the percentage and position of the sealing deposits  
452 in specimen kept in seawater for 1, 3, and 7 weeks.
- 453 Fig. 12. Temporal change of the percentage of the sealing deposits for specimen  
454 kept in seawater for 1, 3, and 7 weeks.

455 **Table legends**

456

457 Table 1. Composition of HSULPC (after Nara et al. [13]).

458 Table 2. Chemical composition of simulated seawater (mol/L).

459 **Tables**

460

461 Table 1. Composition of HSULPC (after Nara et al. [13]).

462

Amount [kg/m <sup>3</sup> ]	
Low-heat Portland cement	744 – 1014
Silica fume	158 – 496
Fillers (fly ash, blast furnace slag, etc.)	225 – 541
Aggregates	631 – 947
Water-reducing admixture	24
Water	180

463

464

465

466 Table 2. Chemical composition of simulated seawater (mol/L).

467

Ca <sup>2+</sup>	10×10 <sup>-3</sup>
SO <sub>3</sub> <sup>2-</sup>	29×10 <sup>-3</sup>
Na <sup>+</sup>	45×10 <sup>-2</sup>
K <sup>+</sup>	19×10 <sup>-3</sup>
Cl <sup>-</sup>	56×10 <sup>-2</sup>
Mg <sup>2+</sup>	55×10 <sup>-3</sup>
HCO <sub>3</sub> <sup>-</sup>	24×10 <sup>-4</sup>

468

469

470

471

472

473

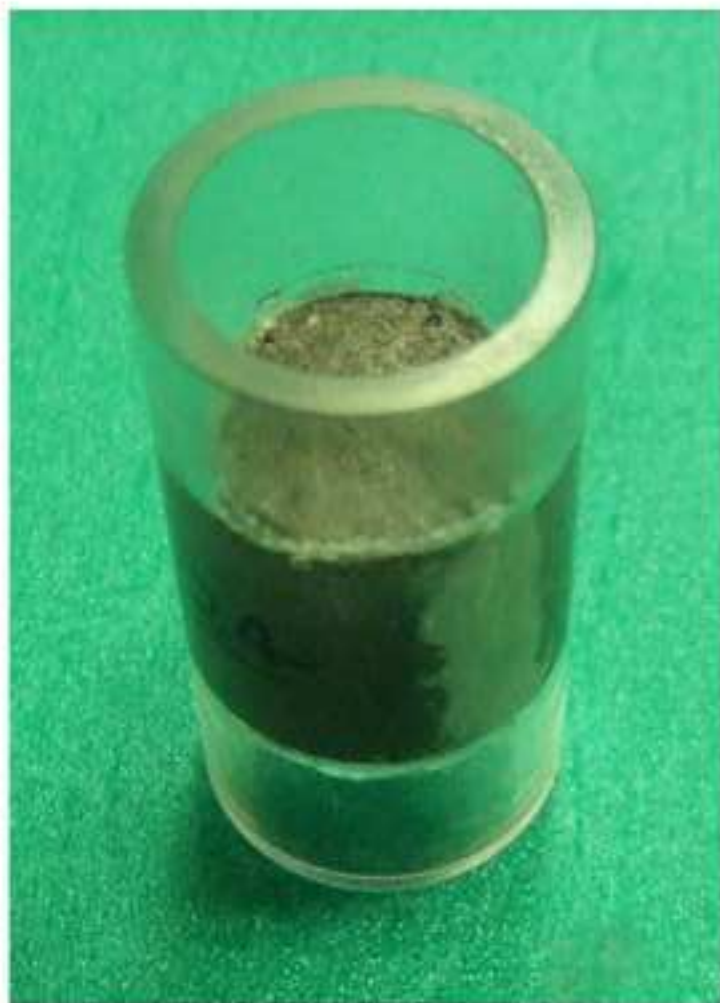
474

475

476

Figure1

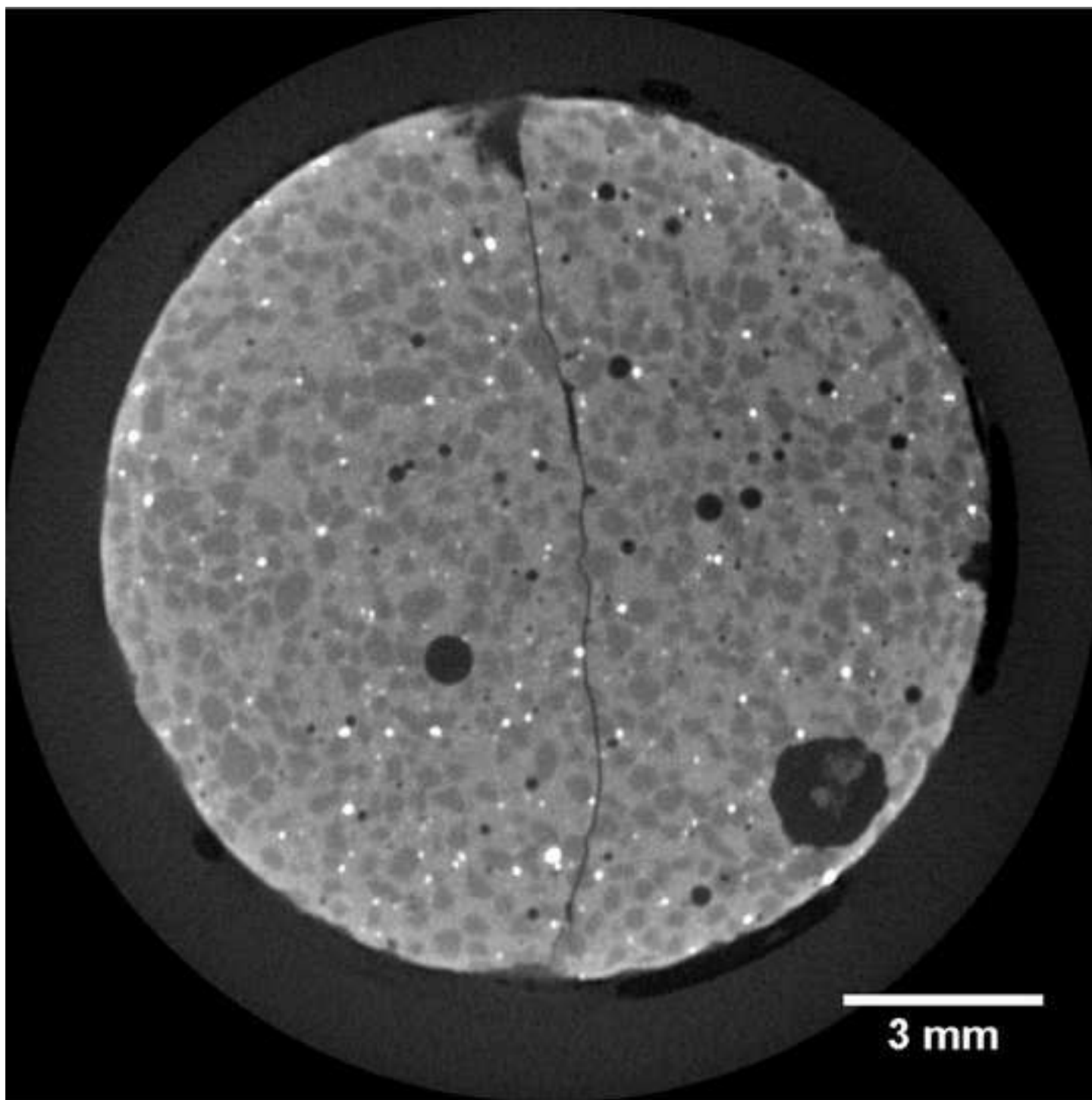
[Click here to download high resolution image](#)

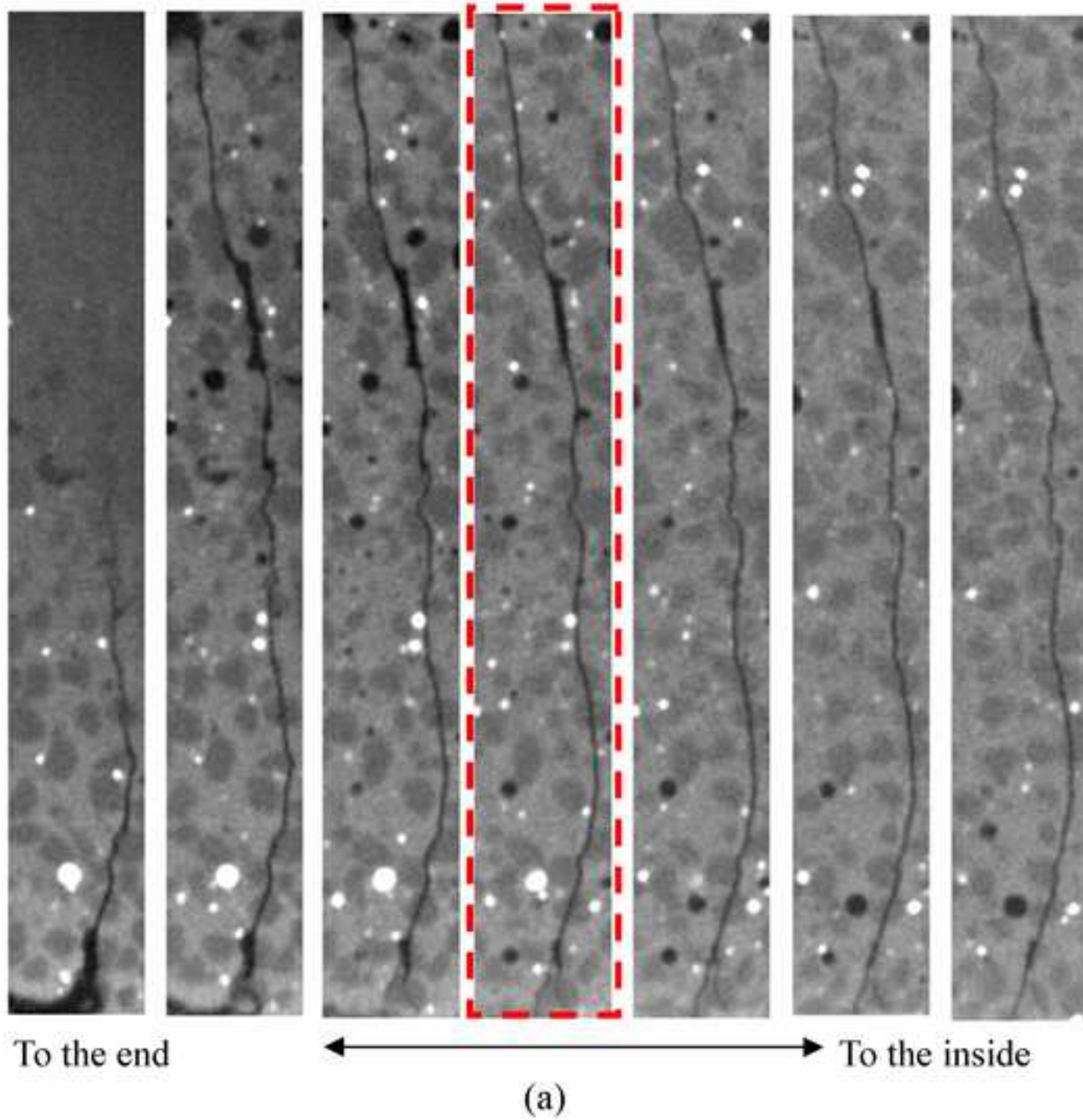


(a)

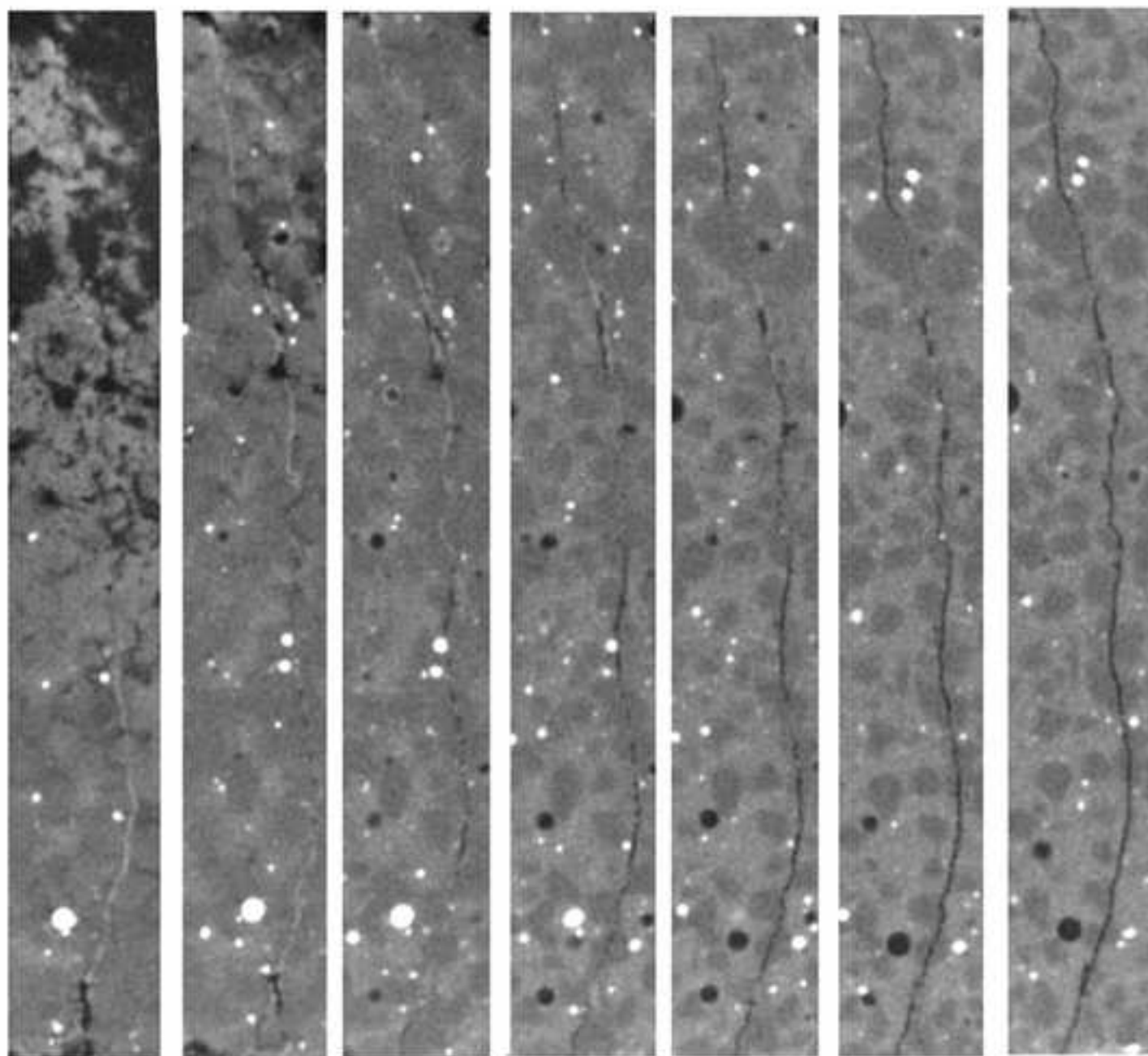


(b)

[Download high resolution image](#)

[Download high resolution image](#)



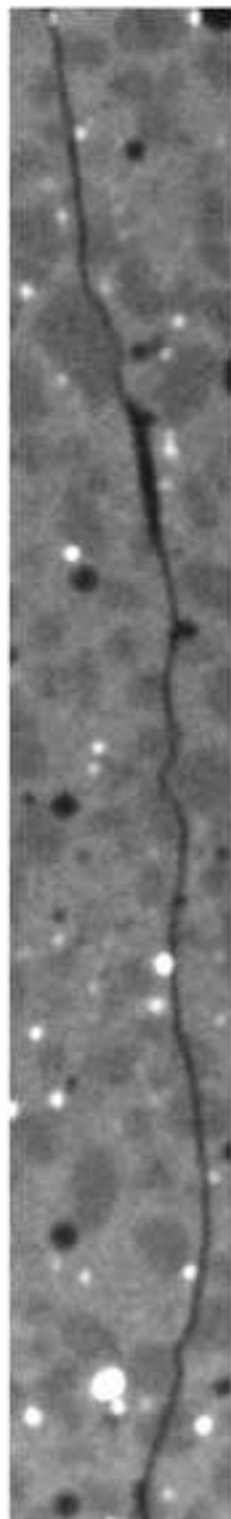
[Download high resolution image](#)

To the end

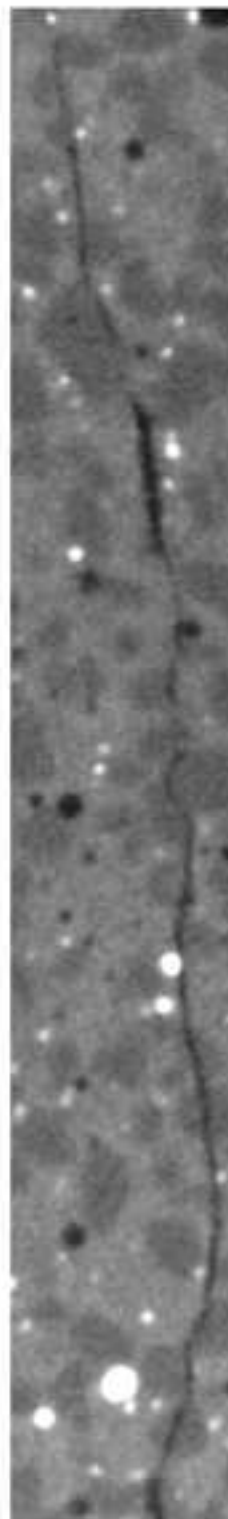
(b)

To the inside



[Download high resolution image](#)

Before  
immersion



1 week

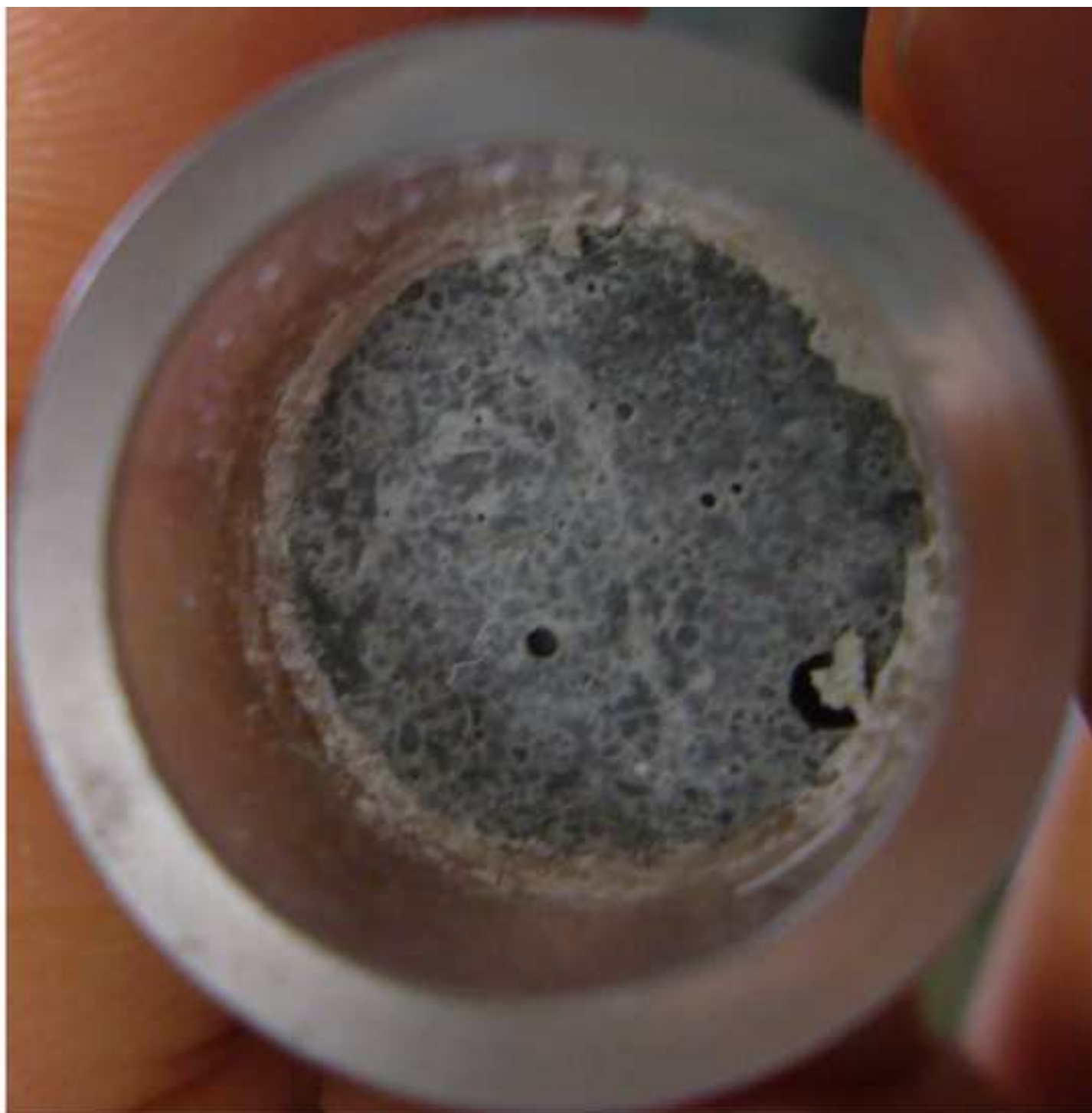


3 weeks



7 weeks

Download high resolution image



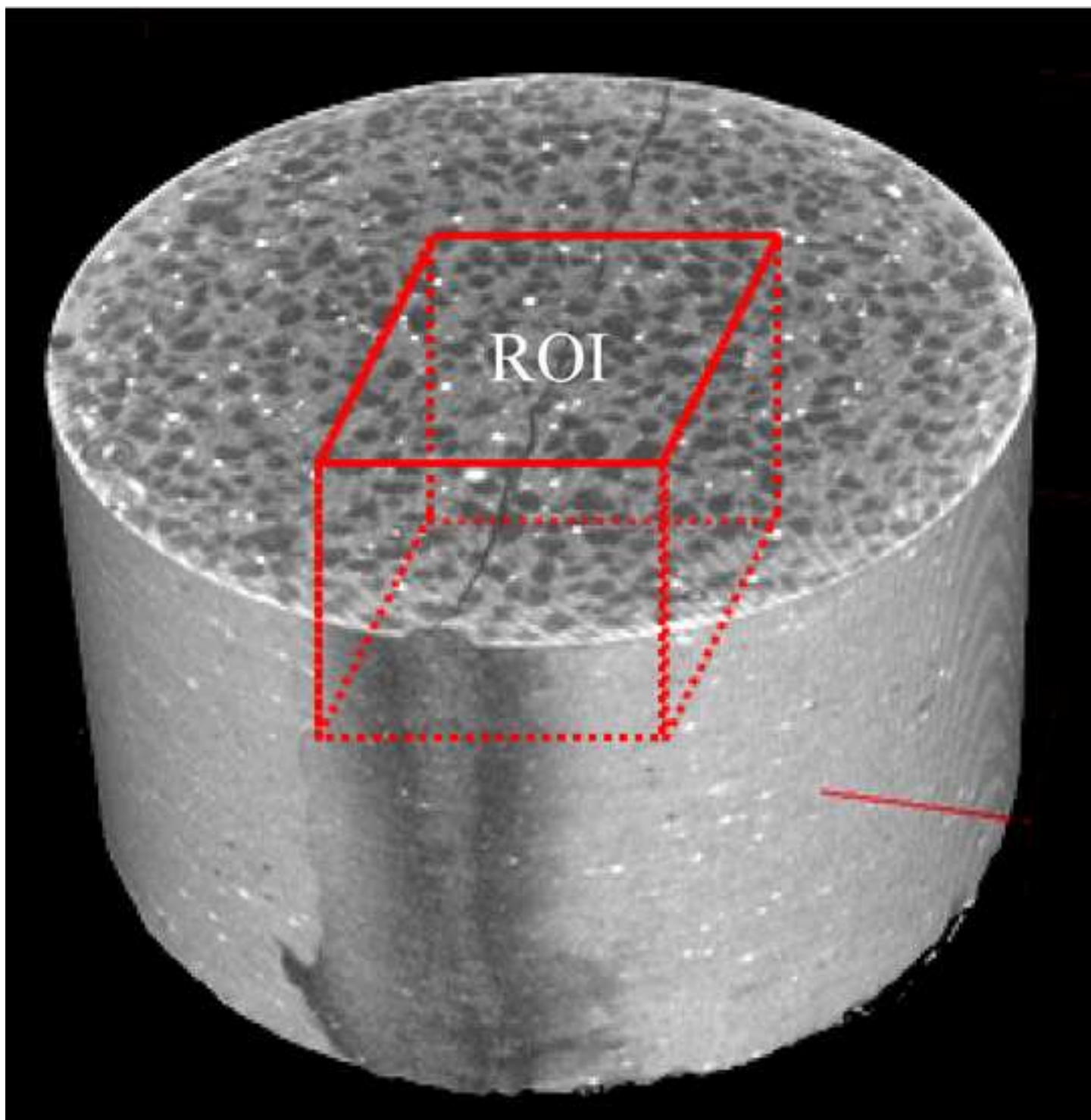
[Download high resolution image](#)



Figure7  
[Click here to download high resolution image](#)

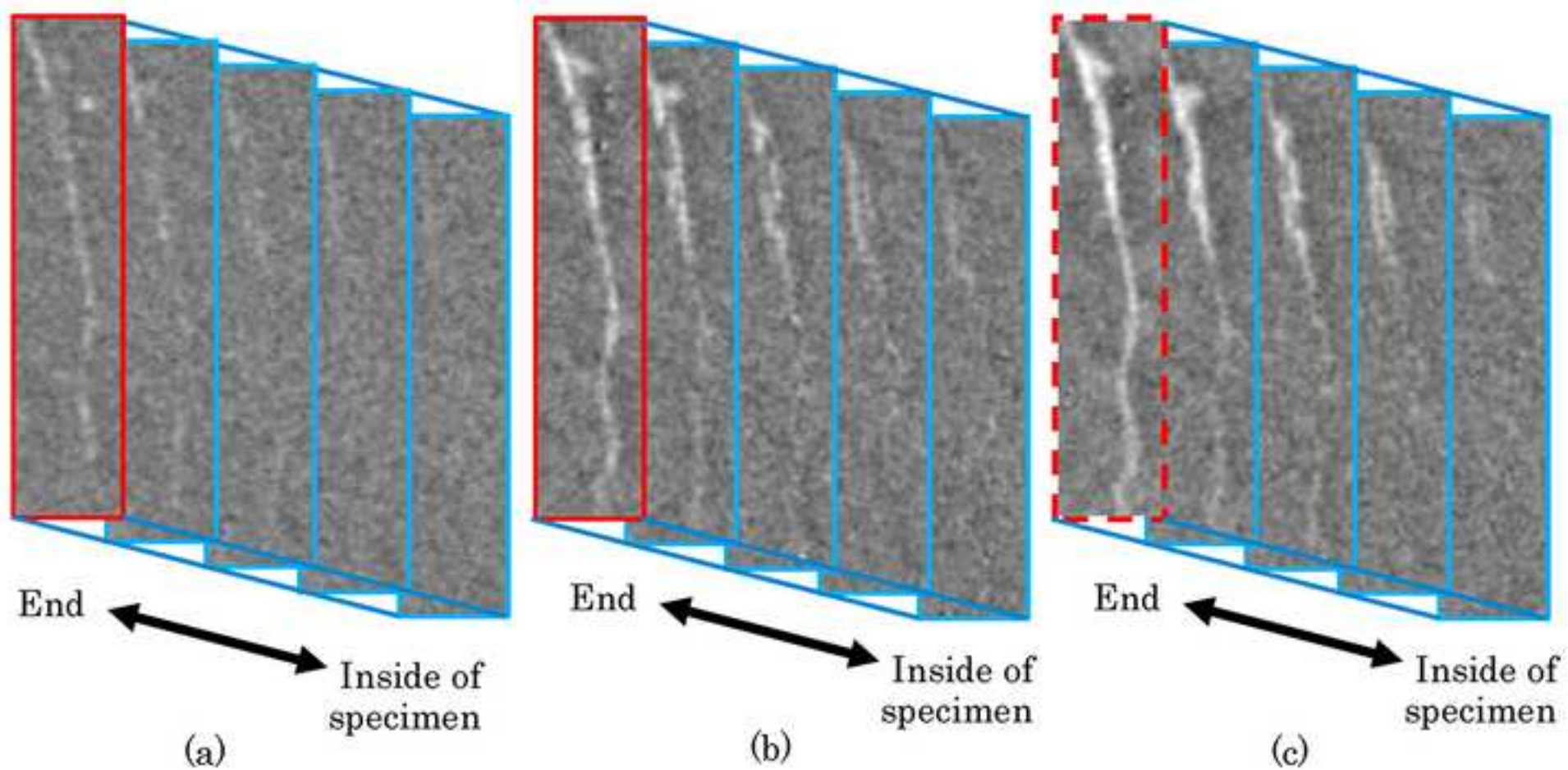
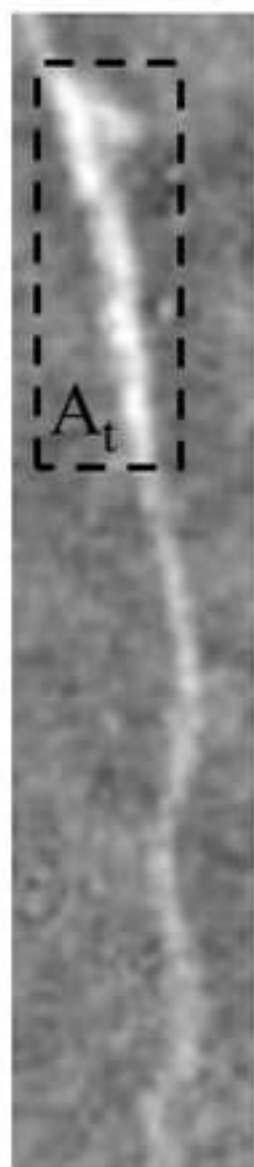
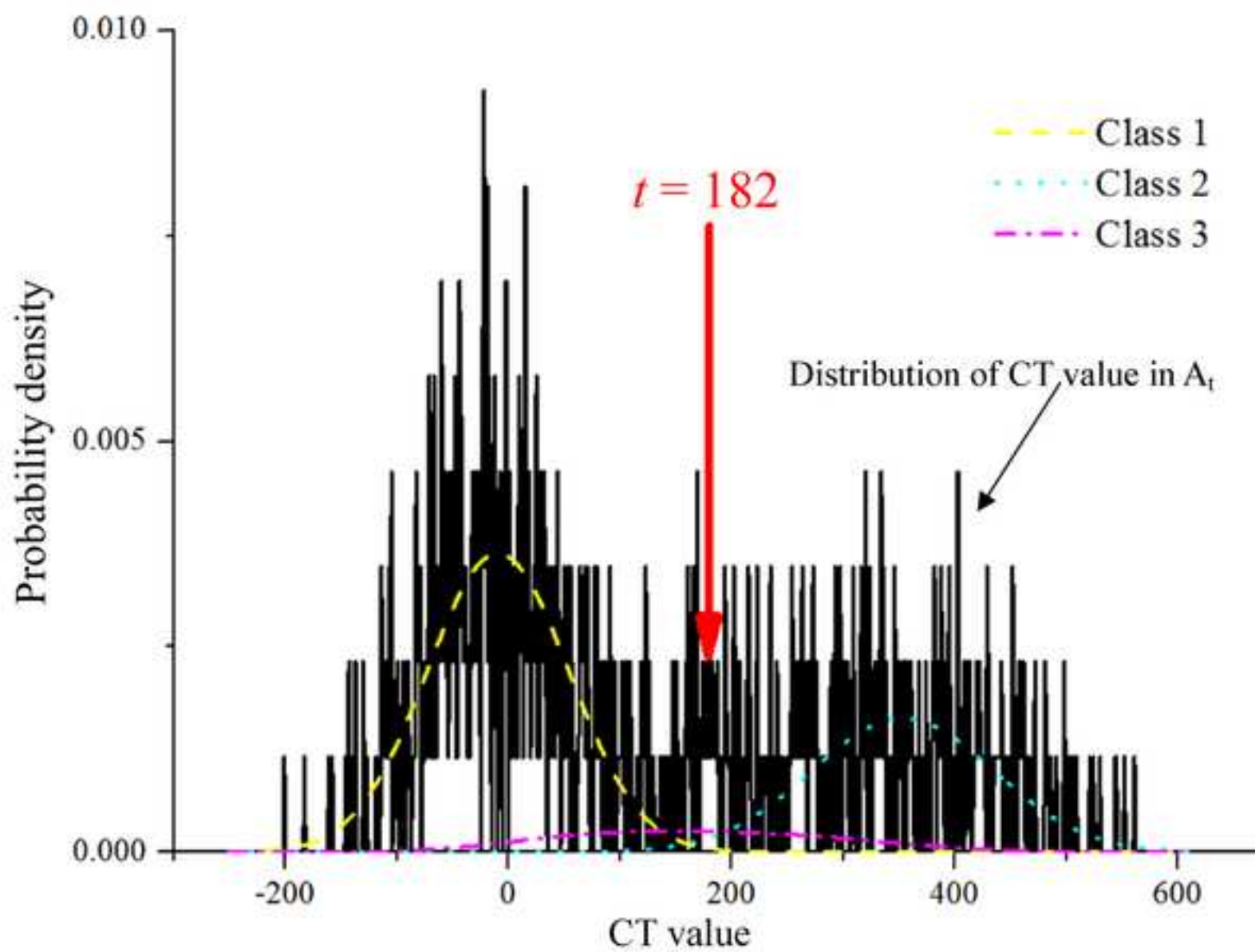


Figure8  
[Click here to download high resolution image](#)

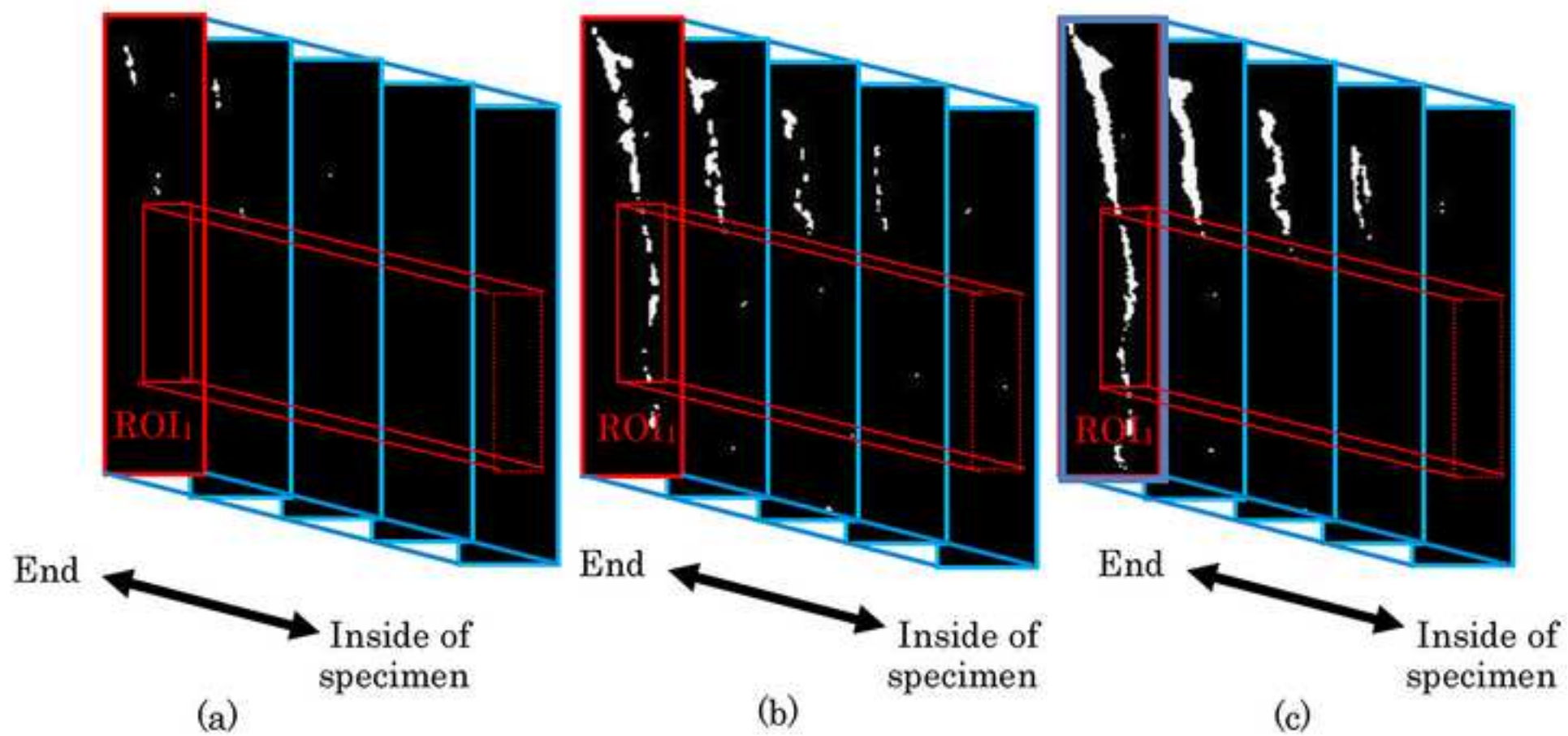


(a)



(b)

Figure9  
[Click here to download high resolution image](#)



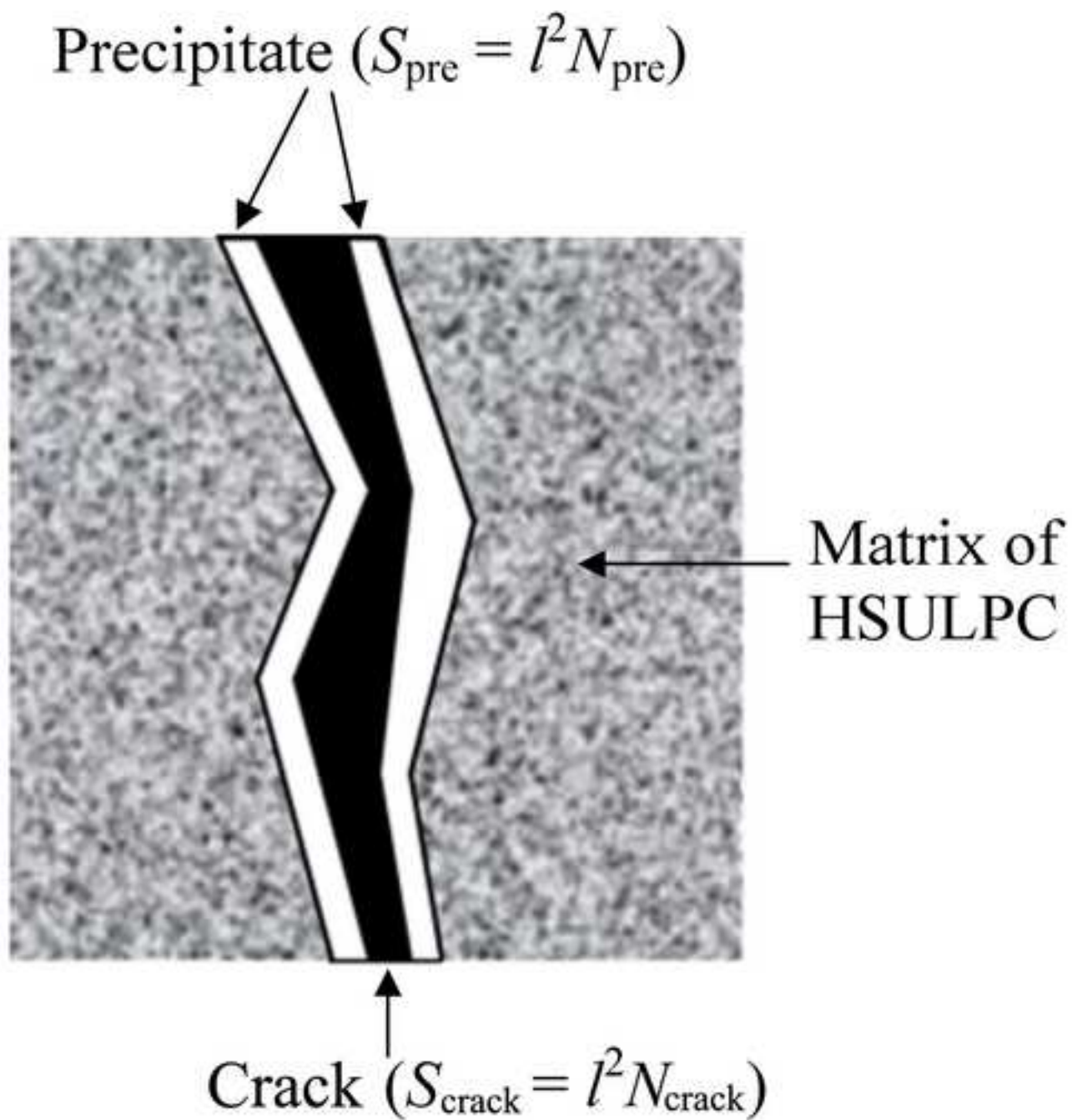




Figure11  
[Click here to download high resolution image](#)

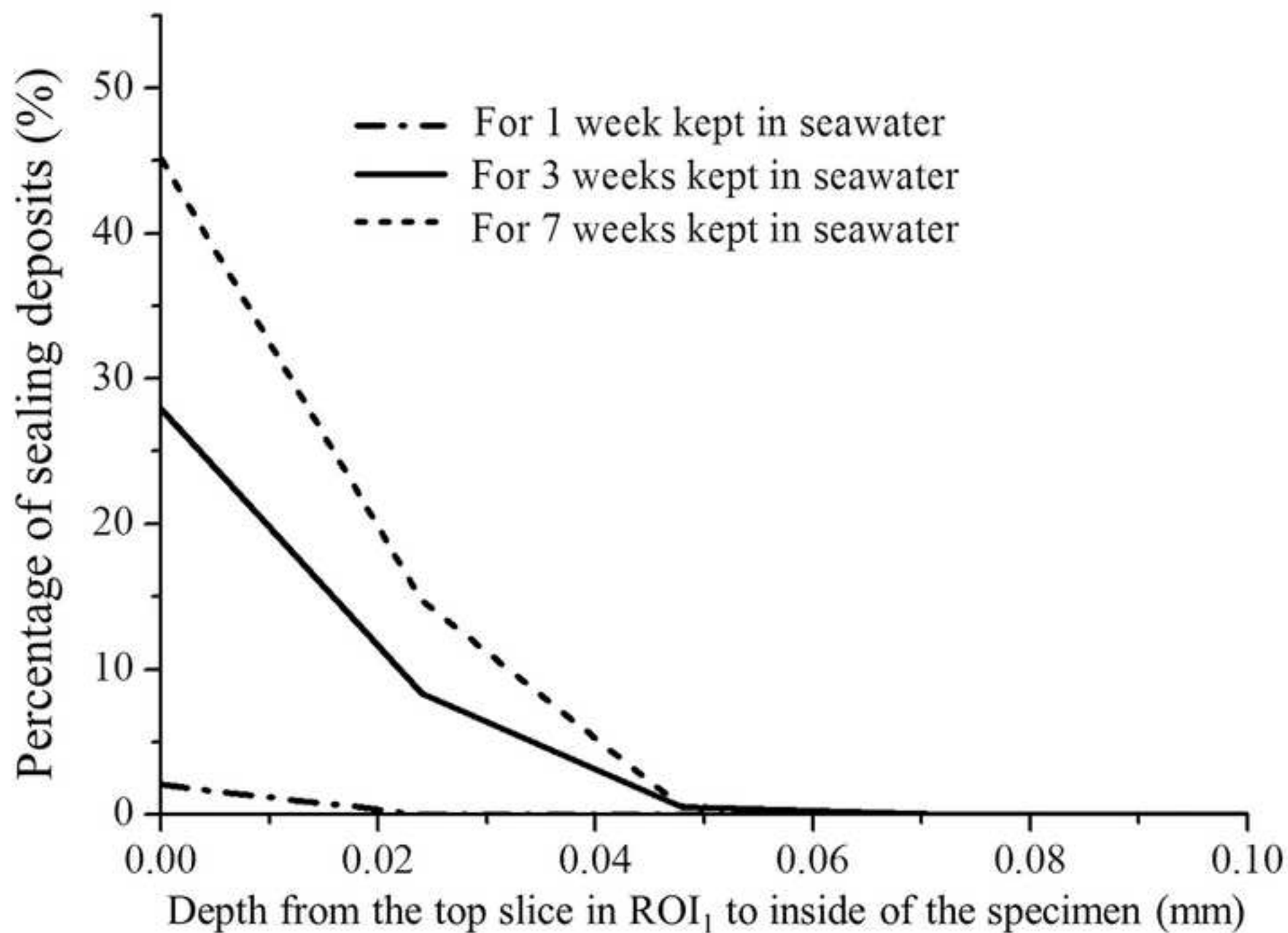




Figure12

[Click here to download high resolution image](#)

